BasicVSR++: Improving Video Super-Resolution with Enhanced Propagation and Alignment

Kelvin C.K. Chan Shangchen Zhou Xiangyu Xu Chen Change Loy✉
S-Lab, Nanyang Technological University
{chan0899, s200094, xiangyu.xu, ccloy}@ntu.edu.sg

2022 IEEE/CVF Conference on Computer Vision and Pattern Recognition (CVPR) | 978-1-6654-6946-3/22/$31.00 ©2022 IEEE | DOI: 10.1109/CVPR52688.2022.00588

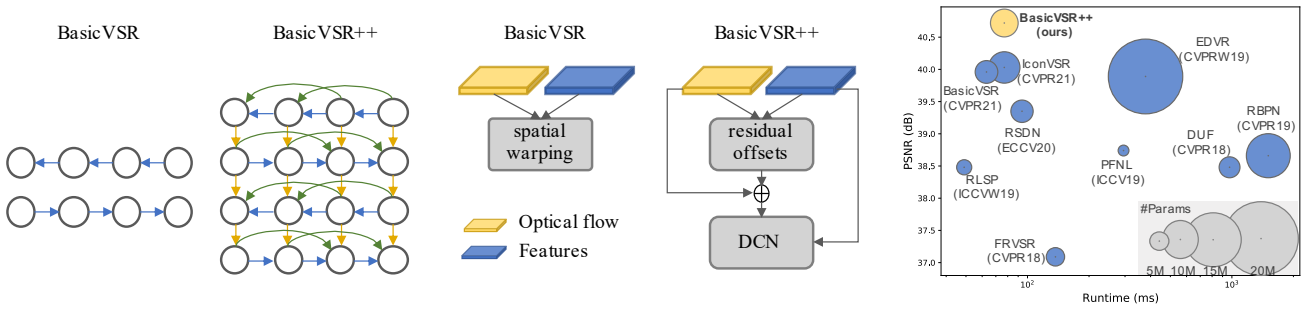

(a) Propagation (b) Alignment (c) Performance Gain

Figure 1. **Improvements over BasicVSR [3]. (a)** Second-order grid propagation in BasicVSR++ allows a more effective propagation of features. **(b)** Flow-guided deformable alignment in BasicVSR++ provides a means for more robust feature alignment across misaligned frames. **(c)** BasicVSR++ outperforms existing state of the arts including its predecessor, BasicVSR, while maintaining efficiency.

Abstract

A recurrent structure is a popular framework choice for the task of video super-resolution. The state-of-the-art method BasicVSR adopts bidirectional propagation with feature alignment to effectively exploit information from the entire input video. In this study, we redesign BasicVSR by proposing second-order grid propagation and flow-guided deformable alignment. We show that by empowering the recurrent framework with enhanced propagation and alignment, one can exploit spatiotemporal information across misaligned video frames more effectively. The new components lead to an improved performance under a similar computational constraint. In particular, our model BasicVSR++ surpasses BasicVSR by a significant 0.82 dB in PSNR with similar number of parameters. BasicVSR++ is generalizable to other video restoration tasks, and obtains three champions and one first runner-up in NTIRE 2021 video restoration challenge.

1. Introduction

Video super-resolution (VSR) is challenging in that one needs to gather complementary information across misaligned video frames for restoration. One prevalent approach is the sliding-window framework [9, 28, 31, 35], where each frame in the video is restored using the frames within a short temporal window. In contrast to the sliding-window framework, a recurrent framework attempts to exploit the long-term dependencies by propagating the latent features. In general, these methods [8, 10–12, 14, 24] allow a more compact model compared to those in the sliding-window framework. Nevertheless, the problems of transmitting long-term information and aligning features across frames in a recurrent model remain challenging.

We study the problems above by choosing the recent state of the art, BasicVSR [3], as our base model. Improving BasicVSR is non-trivial because it has already been used to explore different schemes and is one of the most effective designs for feature propagation and alignment. In particular, BasicVSR adopts bidirectional propagation to aggressively exploit information from the entire input video for reconstruction. For alignment, it designs an effective module that uses optical flow for feature warping (see Fig. 1).

We wish to explore if there are more effective ways to aggregate temporal information in a video, so that one can restore finer details and deal with occluded and complex regions better than BasicVSR. Such a study is meaningful and fundamental as it will benefit the design of future VSR models. To this end, we redesign BasicVSR by devising *second-order grid propagation* and *flow-guided deformable alignment* that allow information to be propagated and aggregated more effectively.

978-1-6654-6946-3/22/$31.00 ©2022 IEEE
DOI 10.1109/CVPR52688.2022.00588

While the basic backbone and structure of our network is inspired by BasicVSR (so as to allow fair comparisons), our two components are novel. No previous literature has explored the notion of grid-like second-order propagation and flow-guided deformable alignment. In particular,

1) The proposed second-order grid propagation, as shown in Fig. 1(a), addresses two limitations in exiting recurrent VSR networks: i) we allow more aggressive bidirectional propagation arranged in a grid-like manner, and ii) we relax the assumption of first-order Markov property, and incorporate a second-order connection into the network so that information can be aggregated from different spatiotemporal locations. Both modifications ameliorate information flow in the network and improve robustness of the network against occluded and fine regions.

2) Inaccurate flow estimation could jeopardize the restoration performance. Deformable alignment [28, 29, 31] has demonstrated its superiority in VSR, but it is difficult to train in practice [4]. To take advantage of deformable alignment while overcoming the training instability, we propose flow-guided deformable alignment, as shown in Fig. 1(b). In the proposed module, instead of learning the DCN offsets directly [6, 39], we reduce the burden of offset learning by using optical flow field as base offsets refined by flow field residue. The latter can be learned more stably than the original DCN offsets.

Enhanced by the above design improvements, BasicVSR++ can adopt a more lightweight backbone than its counterparts: BasicVSR++ surpasses existing state of the arts by a large margin while maintaining efficiency (Fig. 1(c)). In particular, when compared to its predecessor BasicVSR, a considerable gain of 0.82 dB in PSNR on REDS4 [31] is obtained with similar numbers of parameters. We show that the proposed components can further benefit other video restoration tasks such as compressed video enhancement and real-world VSR.

2. Related Work

Recurrent Networks. The recurrent framework is a popular structure adopted in various video processing tasks such as super-resolution [8, 10–12, 14, 24], deblurring [22, 38], and frame interpolation [33]. For instance, RSDN [12] adopts unidirectional propagation with a recurrent detail structural block and a hidden state adaptation module to enhance the robustness to appearance change and error accumulation. Chan *et al*. [3] propose BasicVSR, demonstrating the importance of bidirectional propagation over unidirectional propagation to better exploit features temporally. In addition, the study also shows the advantage of feature alignment in aligning highly relevant but misaligned features. We refer readers to [3] for the detailed comparisons of these components against the conventional ways of performing propagation and alignment. In this paper, we show a more effective way than that of BasicVSR for harnessing temporal information and present a novel way of synergizing optical flow and deformable alignment.

Grid Connections. Grid-like designs are seen in various vision tasks such as object detection [26, 30], semantic segmentation [7, 26, 30, 40], and frame interpolation [23]. In general, these designs decompose a given image/feature into multiple resolutions, and grids are adopted *across resolutions* to capture both fine and coarse information. Unlike aforementioned methods, BasicVSR++ does not adopt a multi-scale design. Instead, the grid structure is designed for propagation *across time* in a bidirectional fashion. We link different frames with a grid connection to repeatedly refine the features, improving expressiveness.

Higher-Order Propagation. Higher-order propagation has been studied to improve gradient flow [16, 18, 25]. These methods demonstrate improvements in different tasks including classification [16] and language modeling [25]. However, these methods do not consider temporal alignment, which has shown to be critical in the VSR task [3]. To allow temporal alignment in second-order propagation, we incorporate alignment into our propagation scheme by extending our flow-guided deformable alignment to the second-order settings.

Deformable Alignment. TDAN [28] performs alignment at the feature level using deformable convolution. EDVR [31] further proposes a Pyramid Cascading Deformable (PCD) alignment with a multi-scale design. Recently, Chan *et al*. [4] analyze deformable alignment and show that the performance gain over flow-based alignment comes from the offset diversity. Motivated by [4], we adopt deformable alignment but with a reformulation to overcome the training instability [4]. Our flow-guided deformable alignment is different from offset-fidelity loss [4]. The latter uses optical flow as a loss function during training. In contrast, we directly incorporate optical flow into our module as base offsets, allowing a more explicit guidance, both during training and inference.

3. Methodology

BasicVSR++ consists of two effective redesigns for improving *propagation* and *alignment*. As depicted in Fig. 2, given an input video, residual blocks are first applied to extract features from each frame. The features are then propagated using our second-order grid propagation scheme, where alignment is performed by the newly proposed flow-guided deformable alignment. After propagation, the aggregated features are used to generate the output image through convolution and pixel-shuffling.

3.1. Second-Order Grid Propagation

Most existing methods adopt unidirectional propagation [12, 14, 24]. Several works [3, 10, 11] adopt bidirectional

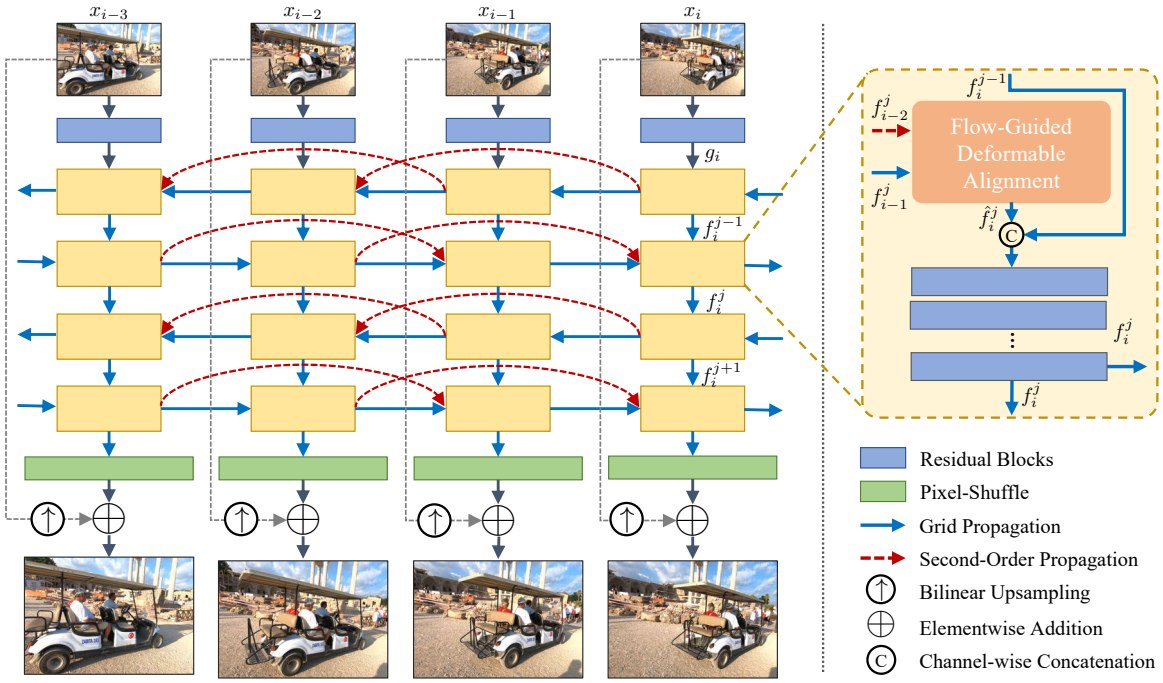

Figure 2. **An Overview of BasicVSR++.** BasicVSR++ consists of two redesigns to improve propagation and alignment in its predecessor BasicVSR [3]. For propagation, we introduce grid propagation (blue solid lines) to refine features bidirectionally. In addition, second-order connection (red dotted lines) is adopted to improve the robustness of propagation. Within each propagation branch, flow-guided deformable alignment is proposed to increase the offset diversity while overcoming the offset overflow problem.

propagation for exploiting the information available in the video sequence. In particular, IconVSR (the more powerful variant of BasicVSR) [3] consists of a coupled propagation scheme with sequentially-connected branches to facilitate information exchange.

To improve bidirectional propagation further, we devise a grid propagation scheme to enable *repeated refinement through propagation*. More specifically, the intermediate features are propagated backward and forward in time in an alternating manner. Through propagation, the information from different frames can be "revisited" and adopted for feature refinement. Compared to existing works, e.g., BasicVSR, which propagate features only once, grid propagation repeatedly extracts information from the entire sequence, improving feature expressiveness.

To further enhance the robustness of propagation, we relax the assumption of first-order Markov property in BasicVSR and adopt a second-order connection, realizing a second-order Markov chain. With this relaxation, information can be aggregated from different spatiotemporal locations, improving robustness and effectiveness in occluded and fine regions.

Through integrating the above two components, we devise our second-order grid propagation as follows. Let x_i be the input image, g_i be the feature extracted from x_i by multiple residual blocks, and f_i^j be the feature computed at the i-th timestep in the j-th propagation branch. In this section, we only describe the formulation for forward propagation. The procedure for backward propagation can be defined similarly.

To compute the feature f_i^j, we first align f_{i-1}^j and f_{i-2}^j following the second-order Markov chain using our proposed flow-guided deformable alignment (discussed in the next section):

$$\hat{f}_i^j = \mathcal{A}\left(g_i, f_{i-1}^j, f_{i-2}^j, s_{i\to i-1}, s_{i\to i-2}\right), \tag{1}$$

where $s_{i\to i-1}, s_{i\to i-2}$ denote the optical flows from i-th frame to the $(i-1)$-th and $(i-2)$-th frames, respectively, and $\mathcal{A}$ represents flow-guided deformable alignment[1]. The features are then concatenated and passed into a stack of residual blocks:

$$f_i^j = \hat{f}_i^j + \mathcal{R}\left(c\left(f_i^{j-1}, \hat{f}_i^j\right)\right), \tag{2}$$

where $f_i^0 = g_i$, $\mathcal{R}$ denotes the residual blocks, and c denotes concatenation along channel dimension.

3.2. Flow-Guided Deformable Alignment

BasicVSR [3] adopts optical flows for feature warping. In our redesign, we synergize optical flow and deformable

[1] $s_{0\to-1}{=}s_{0\to-2}{=}s_{1\to-1}{=}f_{-1}{=}f_{-2}{=}0$.

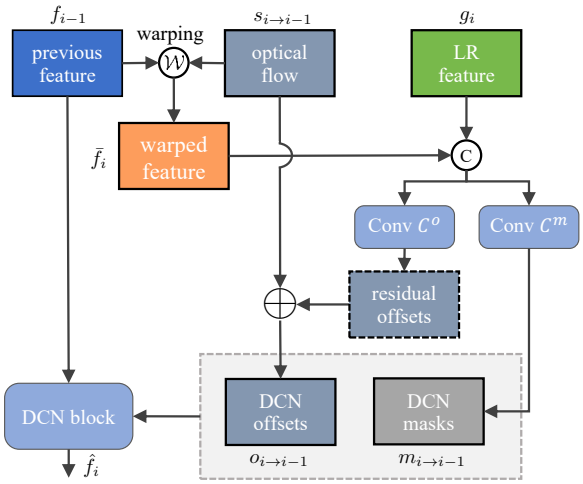

Figure 3. **Flow-guided deformable alignment.** Optical flow is used to pre-align the features. The aligned features are then concatenated to produce the DCN offsets (residue to optical flow). A DCN is then applied to the unwarped features. Only first-order connections are depicted for simplicity.

alignment for improved feature alignment. Deformable alignment [29, 31] has demonstrated significant improvements over flow-based alignment [9, 35] thanks to the offset diversity [4] intrinsically introduced in deformable convolution (DCN) [6, 39]. However, deformable alignment module can be difficult to train [4]. The training instability often results in offset overflow, deteriorating the final performance.

To take advantage of the offset diversity while overcoming the instability, we propose to employ optical flow to guide deformable alignment, motivated by the strong relation between deformable alignment and flow-based alignment [4]. The graphical illustration is shown in Fig. 3. In the rest of this section, we detail the alignment procedure for forward propagation. The procedure for backward propagation is defined similarly. The superscript j is omitted for notational simplicity.

At the i-th timestep, given the feature g_i computed from the i-th LR image, the feature f_{i-1} computed for the previous timestep, and the optical flow $s_{i\to i-1}$ to the previous frame, we first warp f_{i-1} with $s_{i\to i-1}$:

$$\bar{f}_{i-1} = \mathcal{W}(f_{i-1}, s_{i\to i-1}), \tag{3}$$

where $\mathcal{W}$ denotes the spatial warping operation. The pre-aligned features are then used to compute the DCN offsets $o_{i\to i-1}$ and modulation masks $m_{i\to i-1}$. Instead of directly computing the DCN offsets, we compute the residue to the optical flow:

$$\begin{aligned} o_{i\to i-1} &= s_{i\to i-1} + \mathcal{C}^o\left(c(g_i, \bar{f}_{i-1})\right), \\ m_{i\to i-1} &= \sigma\left(\mathcal{C}^m\left(c(g_i, \bar{f}_{i-1})\right)\right). \end{aligned} \tag{4}$$

Here $\mathcal{C}^{\{o,m\}}$ denotes a stack of convolutions, and σ denotes the sigmoid function. A DCN is then applied to the unwarped feature f_{i-1}:

$$\hat{f}_i = \mathcal{D}\left(f_{i-1}; o_{i\to i-1}, m_{i\to i-1}\right), \tag{5}$$

where $\mathcal{D}$ denotes a deformable convolution.

The above formulation is designed only for aligning one single feature, and hence is not directly applicable to our second-order propagation. The most intuitive way to adapt to the second-order setting is to apply the above procedure to the two features, f^j_{i-1} and f^j_{i-2} independently. However, this requires doubled computations, resulting in reduced efficiency. Furthermore, separate alignment potentially ignores the complementary information from the features. Therefore, we allow alignment of two features simultaneously. More specifically, we concatenate the warped features and flows to compute the offsets o_{i-p} (p=1, 2):

$$\begin{aligned} o_{i\to i-p} &= s_{i\to i-p} + \mathcal{C}^o\left(c(g_i, \bar{f}_{i-1}, \bar{f}_{i-2})\right), \\ m_{i\to i-p} &= \sigma\left(\mathcal{C}^m\left(c(g_i, \bar{f}_{i-1}, \bar{f}_{i-2})\right)\right). \end{aligned} \tag{6}$$

A DCN is then applied to the unwarped features:

$$\begin{aligned} o_i &= c(o_{i\to i-1}, o_{i\to i-2}), \\ m_i &= c(m_{i\to i-1}, m_{i\to i-2}), \\ \hat{f}_i &= \mathcal{D}\left(c(f_{i-1}, f_{i-2}); o_i, m_i\right). \end{aligned} \tag{7}$$

More details of the second-order flow-guided deformable alignment are provided in the supplementary material.

Discussion. Unlike existing methods [28, 29, 31, 34] that directly compute the DCN offsets, our proposed flow-guided deformable alignment adopts optical flow as guidance. The benefits are two-fold. First, the learning of offsets can be assisted by pre-aligning the features using optical flow. Second, by learning only the residue, the network needs to learn only small deviations from the optical flow, reducing the burden in typical deformable alignment modules. In addition, instead of directly concatenating the warped feature, the modulation masks in DCN act as attention maps to weigh the contributions of different pixels, providing additional flexibility.

4. Experiments

Two widely-used datasets are adopted for training: REDS [21] and Vimeo-90K [35]. For REDS, following BasicVSR [3], we use REDS4[2] as our test set and REDSval4[3] as our validation set. The remaining clips are used for training. We use Vid4 [19], UDM10 [37], and Vimeo-90K-T [35] as test sets along with Vimeo-90K. All models are tested with 4× downsampling using two degradations –

[2]Clips 000, 011, 015, 020 of REDS training set.
[3]Clips 000, 001, 006, 017 of REDS validation set.

Table 1. **Quantitative comparison (PSNR/SSIM).** All results are calculated on Y-channel except REDS4 [21] (RGB-channel). **Green** and blue colors indicate the best and the second-best performance, respectively. The runtime is computed on an LR size of 180×320. A 4× upsampling is performed following previous studies. Blank entries correspond to results that are not reported in previous works.

			BI degradation			BD degradation		
	Params (M)	Runtime (ms)	REDS4 [21]	Vimeo-90K-T [35]	Vid4 [19]	UDM10 [37]	Vimeo-90K-T [35]	Vid4 [19]
Bicubic	-	-	26.14/0.7292	31.32/0.8684	23.78/0.6347	28.47/0.8253	31.30/0.8687	21.80/0.5246
VESPCN [1]	-	-	-	-	25.35/0.7557	-	-	-
SPMC [27]	-	-	-	-	25.88/0.7752	-	-	-
TOFlow [35]	-	-	27.98/0.7990	33.08/0.9054	25.89/0.7651	36.26/0.9438	34.62/0.9212	-
FRVSR [24]	5.1	137	-	-	-	37.09/0.9522	35.64/0.9319	26.69/0.8103
DUF [15]	5.8	974	28.63/0.8251	-	-	38.48/0.9605	36.87/0.9447	27.38/0.8329
RBPN [9]	12.2	1507	30.09/0.8590	37.07/0.9435	27.12/0.8180	38.66/0.9596	37.20/0.9458	-
EDVR-M [31]	3.3	118	30.53/0.8699	37.09/0.9446	27.10/0.8186	39.40/0.9663	37.33/0.9484	27.45/0.8406
EDVR [31]	20.6	378	31.09/0.8800	37.61/0.9489	27.35/0.8264	39.89/0.9686	37.81/0.9523	27.85/0.8503
PFNL [37]	3.0	295	29.63/0.8502	36.14/0.9363	26.73/0.8029	38.74/0.9627	-	27.16/0.8355
MuCAN [17]	-	-	30.88/0.8750	37.32/0.9465	-	-	-	-
TGA [13]	5.8	-	-	-	-	-	37.59/0.9516	27.63/0.8423
RLSP [8]	4.2	49	-	-	-	38.48/0.9606	36.49/0.9403	27.48/0.8388
RSDN [12]	6.2	94	-	-	-	39.35/0.9653	37.23/0.9471	27.92/0.8505
RRN [14]	3.4	45	-	-	-	38.96/0.9644	-	27.69/0.8488
BasicVSR [3]	6.3	63	31.42/0.8909	37.18/0.9450	27.24/0.8251	39.96/0.9694	37.53/0.9498	27.96/0.8553
IconVSR [3]	8.7	70	31.67/0.8948	37.47/0.9476	27.39/0.8279	40.03/0.9694	37.84/0.9524	28.04/0.8570
VSR-Tran [2]	32.6	4312	31.06/0.8815	37.71/0.9494	27.36/0.8258	-	-	-
BasicVSR++	7.3	77	**32.39/0.9069**	**37.79/0.9500**	**27.79/0.8400**	**40.72/0.9722**	**38.21/0.9550**	**29.04/0.8753**

Bicubic (BI) and Blur Downsampling (BD). More detailed settings are provided in the supplementary material. Code and models have been released to MMEditing [20].

4.1. Comparisons with State-of-the-Art Methods

We conduct comprehensive experiments by comparing with 17 models, as listed in Table 1. The quantitative results are summarized in Table 1 and the speed and performance comparison is provided in Fig. 1(c). For fair comparison, note that the parameters reported above are inclusive of that in the optical flow network (if any).

As shown in Table 1, BasicVSR++ achieves state-of-the-art performance on all datasets for both degradations. In particular, BasicVSR++ outperforms EDVR [31], a large-capacity sliding-window method, by up to 1.3 dB in PSNR, while having 65% fewer parameters. BasicVSR++ also outperforms the recent Transformer-based method [2] with 78% fewer parameters and 18× faster speed. When compared to the previous state of the art, IconVSR [3], BasicVSR++ both possesses fewer parameters and shows improvements of up to 1 dB. As shown in Table 2, even if we train a lighter version of BasicVSR++ (denoted as Light-BasicVSR++) with comparable network parameters and runtime to BasicVSR and IconVSR, our model still shows an improvement of 0.82 dB over BasicVSR and 0.57 dB over IconVSR. Such gains are considered significant in VSR. For reference, the predecessor BasicVSR only improved over EDVR by 0.33 dB on the same dataset.

From the qualitative comparisons shown in Fig. 4 and Fig. 5, we observe finer details restored by BasicVSR++ compared to other methods. In particular, BasicVSR++ is the only method that recovers the wheel's spokes in Fig. 4 and the stairs in Fig. 5. More examples are provided in the supplementary material.

Table 2. **Performance of a lighter BasicVSR++.** Our lighter model, Light-BasicVSR++, has a similar complexity to BasicVSR and IconVSR, but still shows considerable improvements. The PSNR and runtime are computed on REDS4.

	BasicVSR [3]	IconVSR [3]	**Light-BasicVSR++**
Params (M)	6.3	8.7	6.4
Runtime (ms)	63	70	69
PSNR (dB)	31.42	31.67	**32.24**

We further compare the performance of BasicVSR and BasicVSR++ in occluded regions. With the proposed second-order propagation, BasicVSR++ is able to retrieve information more effectively from farther frames. Our flow-guided deformable alignment further enables BasicVSR++ to extract information more flexibly. It is evident in Fig. 6 that BasicVSR produces blurry outputs when a particular region is occluded in its neighboring frames. In contrast, BasicVSR++ is able to produce clear details by aggregating information from other feasible locations. These fine details cannot be reflected in PSNR, but substantially affect the visual quality of restored frames.

5. Ablation Studies

To understand the contributions of the proposed components, we start with a baseline and gradually insert the components. From Table 3, it is apparent that each component brings considerable improvement, ranging from 0.14 dB to 0.46 dB in PSNR.

The proposed propagation schemes can be extended to

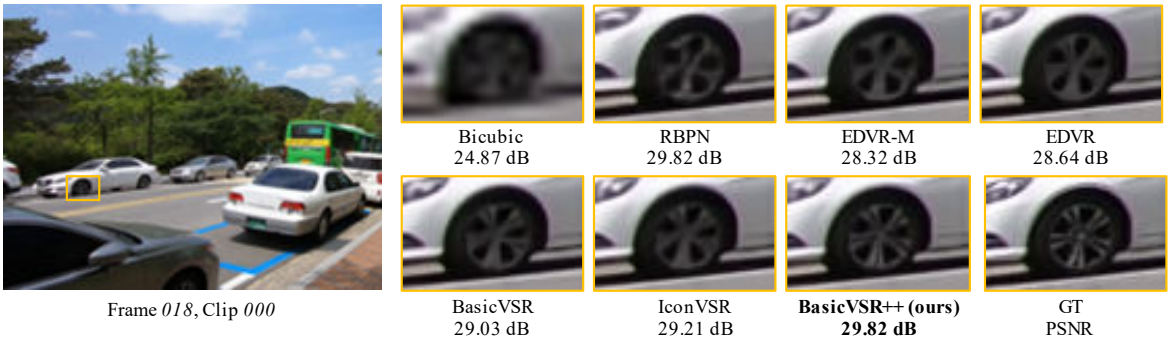

Figure 4. **Challenging scenario on REDS4 [31].** Only BasicVSR++ is able to recover the patterns of the wheel's spokes.

Figure 5. **Challenging scenario on Vimeo-90K-T [35].** Only BasicVSR++ is able to reconstruct the stairs.

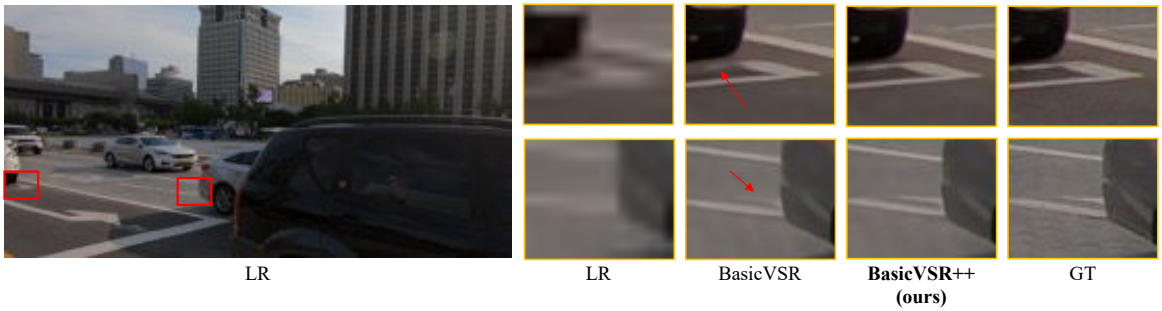

Figure 6. **Performance in occluded regions.** The regions indicated by the red arrows are occluded in two neighboring frames. By employing second-order connections and flow-guided deformable alignment, BasicVSR++ is capable of retrieving information from more potential candidates. **(Zoom-in for best view)**

higher orders and more propagation iterations. However, while the performance gain is considerable when increasing from first-order to second-order (*i.e.*, (B)→(C)), and from one to two iterations (*i.e.*, (C)→BasicVSR++), we observe in our preliminary experiments that further increasing the orders and number of iterations does not lead to a significant improvement (0.05 dB in PSNR) as much information may already be well-captured by the nearest two frames.

Second-Order Grid Propagation. We further provide some qualitative comparisons to understand the contributions of the proposed propagation scheme. As shown in the two examples of Fig. 7, the contribution of both the second-order propagation and grid propagation is more noticeable in regions that contain fine details and complex textures.

Table 3. **Ablation studies.** Each component brings significant improvements in PSNR, verifying their effectiveness.

	(A)	(B)	(C)	**BasicVSR++**
Flow-Guided Deform. Align.		✓	✓	✓
Second-Order Propagation			✓	✓
Grid Propagation				✓
PSNR (dB)	31.48	31.94	32.08	32.39

(a) Second-Order Propagation (b) Grid Propagation

Figure 7. **Benefits of second-order grid propagation.** By propagating the features more effectively, our second-order grid propagation leads to more details, improving the output quality.

(a) Optical flow (b) DCN offsets #1 (c) DCN offsets #2 (d) DCN offsets #3

(e) Reference image (f) Neighboring image (g) Aligned by optical flow (h) Aligned by flow-guided deformable alignment

Figure 8. **Benefits of flow-guided deformable alignment. (a-d)** While DCN offsets are highly similar to optical flow, there are noticeable differences. **(e-f)** The reference and neighboring images. **(g)** The feature aligned by optical flow, as in BasicVSR, experiences blurry edges. **(h)** The feature aligned by our proposed module in BasicVSR++ is sharper and preserves more details, as indicated by the red arrows.

In those regions, there is limited information from the current frame that can be employed for reconstruction. To improve the output quality of those regions, effective information aggregation from other video frames is necessary. With our second-order propagation scheme, the information can be transmitted via a robust and effective propagation. This complementary information essentially assists the restoration of the fine details. As shown in the examples, the network successfully restores the details with our components, whereas the counterparts without our components produce blurry outputs.

Flow-Guided Deformable Alignment. In Fig. 8(a-d), we compare the offsets with the optical flow computed by the flow estimation module in BasicVSR++. By learning only the residue to optical flow, the network produces offsets that are highly similar to the optical flow, but with observable differences. When compared to the baseline which aggregates information from only one spatial location indicated by the motion (optical flow), our proposed module allows retrieving information from multiple locations around, providing additional flexibility.

This flexibility leads to features with better quality, as shown in Fig. 8(g-h). When the warping is performed by using optical flow as in the original BasicVSR, the aligned features contain blurry edges, owing to the interpolation operation in spatial warping. In contrast, by gathering more information from the neighbors, the feature aligned by our proposed module is sharper and preserves more details.

To further demonstrate the superiority of our designs, we compare our alignment module with two variants: (1) No optical flow is used. (2) Optical flow is used as in the offset-fidelity loss [4], *i.e.*, the flow is merely used as supervision in the loss function (rather than serving as base offsets as in our method). As shown in Table 4, without using optical flow as guidance, the instability causes training to collapse, leading to a very poor PSNR value. When using the offset-fidelity loss, the training is stabilized. However, a drop of 2.17 dB from our full model is observed. Our flow-guided deformable alignment directly incorporates optical flow into the network to provide more explicit guidance, leading to better results.

Temporal Consistency. In Fig. 9 we show a comparison of the temporal profiles between BasicVSR++ and two state-of-the-art methods – EDVR and BasicVSR. For the sliding-

Table 4. **Comparison of alignment modules.** Using optical flow to guide deformable alignment successfully stabilizes training. BasicVSR++ directly incorporates optical flow into the network, outperforming the offset-fidelity loss [4].

	w/o Flow	Offset-Fidelity Loss [4]	**Ours**
PSNR (dB)	27.44	30.22	32.39

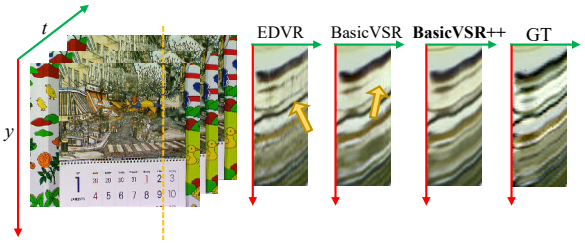

Figure 9. **Comparison of temporal profile.** We select a column (orange dotted lines) and observe the changes across time. The profile from EDVR possesses noise, indicating flickering artifacts. The profile from BasicVSR still contains discontinuity. By better aggregating the long-term information, the profile from BasicVSR++ demonstrates a smoother transition.

window based method EDVR, each frame is reconstructed independently. In such a design, the consistency between the outputs cannot be guaranteed. As a result, its temporal profile contains significant noise, suggesting flickering artifacts in the output video. In contrast, for recurrent networks, without explicit modeling of temporal consistency, the profiles of BasicVSR and BasicVSR++ demonstrate better consistencies. However, the profile of BasicVSR still contains discontinuity. With the benefit of our enhanced propagation and alignment, BasicVSR++ is able to aggregate richer information from video frames, showing smoother temporal transition. The video results are given in the supplementary material.

6. Extended Applications

In addition to non-blind VSR, BasicVSR++ is generalizable to other restoration tasks. In particular, BasicVSR++ achieves **three champions and one first runner-up** in NTIRE 2021 challenge [36]. First, we demonstrate the superiority of BasicVSR++ in compressed video enhancement. From Table 5 we see that BasicVSR++ surpasses the top-ranking teams in the NTIRE 2021 challenge by a large margin. Example outputs are shown in Fig. 10.

We then extend BasicVSR++ to real-world VSR. We keep the architecture unchanged and adopt the second-order degradation model [32] during training. As shown in Fig. 11, with aggressive data augmentation during training, BasicVSR++ is able to generalize to in-the-wild degradations, producing perceptually convincing outputs. In particular, the texts are better recognized and the aliasing is eliminated. However, it is observed that the performance

Table 5. **Performance on compressed video enhancement.** Our BasicVSR++ significantly outperforms the top-ranking methods in the NTIRE 2021 [36] challenge.

	BasicVSR++	Method 1	Method 2	Method 3
PSNR	**30.37**	29.95	29.69	29.64
SSIM	**0.9484**	0.9468	0.9423	0.9405

Figure 10. **Results on compressed video enhancement.** The outputs clearly possesses fewer artifacts, and the details are shown more clearly.

Figure 11. **Results on real-world VSR.** BasicVSR++ is able to remove the unknown degradations, leading to improved quality.

deteriorates when the inputs are severely degraded. More explorations [5] on real-world VSR are left as our future work.

7. Discussion

Our study focuses on addressing the core problems in VSR, namely feature propagation and alignment. The previous state of the art BasicVSR [3], while effective, has not investigated these two components sufficiently. We have shown an effective way beyond the conventional bidirectional propagation to aggregate features from distant frames through grid and second-order connections. With a better aggregation of temporal information, BasicVSR++ obtains a large improvement over its predecessor yet with a similar complexity (Table 2). We have further demonstrated the merits of synergizing optical flow and deformable alignment for aligning different frames. The proposed components are new and generic, meaning that they can be further expanded upon to improve other important video tasks such as deblurring and denoising.

Acknowledgement. This study is supported under the RIE2020 Industry Alignment Fund Industry Collaboration Projects (IAF-ICP) Funding Initiative, as well as cash and in-kind contribution from the industry partner(s). It is also partly supported by the NTU NAP grant.

References

[1] Jose Caballero, Christian Ledig, Aitken Andrew, Acosta Alejandro, Johannes Totz, Zehan Wang, and Wenzhe Shi. Real-time video super-resolution with spatio-temporal networks and motion compensation. In *CVPR*, 2017. 5

[2] Jiezhang Cao, Yawei Li, Kai Zhang, and Luc Van Gool. Video super-resolution transformer. *arXiv preprint arXiv:2106.06847*, 2021. 5

[3] Kelvin C.K. Chan, Xintao Wang, Ke Yu, Chao Dong, and Chen Change Loy. BasicVSR: The search for essential components in video super-resolution and beyond. In *CVPR*, 2021. 1, 2, 3, 4, 5, 8

[4] Kelvin C.K. Chan, Xintao Wang, Ke Yu, Chao Dong, and Chen Change Loy. Understanding deformable alignment in video super-resolution. In *AAAI*, 2021. 2, 4, 7, 8

[5] Kelvin C.K. Chan, Shangchen Zhou, Xiangyu Xu, and Chen Change Loy. Investigating tradeoffs in real-world video super-resolution. In *CVPR*, 2022. 8

[6] Jifeng Dai, Haozhi Qi, Yuwen Xiong, Yi Li, Guodong Zhang, Han Hu, and Yichen Wei. Deformable convolutional networks. In *ICCV*, 2017. 2, 4

[7] Damien Fourure, Rémi Emonet, Élisa Fromont, Damien Muselet, Alain Trémeau, and Christian Wolf. Residual conv-deconv grid network for semantic segmentation. In *BMVC*, 2017. 2

[8] Dario Fuoli, Shuhang Gu, and Radu Timofte. Efficient video super-resolution through recurrent latent space propagation. In *ICCVW*, 2019. 1, 2, 5

[9] Muhammad Haris, Greg Shakhnarovich, and Norimichi Ukita. Recurrent back-projection network for video super-resolution. In *CVPR*, 2019. 1, 4, 5

[10] Yan Huang, Wei Wang, and Liang Wang. Bidirectional recurrent convolutional networks for multi-frame super-resolution. In *NIPS*, 2015. 1, 2

[11] Yan Huang, Wei Wang, and Liang Wang. Video super-resolution via bidirectional recurrent convolutional networks. *TPAMI*, 2018. 1, 2

[12] Takashi Isobe, Xu Jia, Shuhang Gu, Songjiang Li, Shengjin Wang, and Qi Tian. Video super-resolution with recurrent structure-detail network. In *ECCV*, 2020. 1, 2, 5

[13] Takashi Isobe, Songjiang Li, Xu Jia, Shanxin Yuan, Gregory Slabaugh, Chunjing Xu, Ya-Li Li, Shengjin Wang, and Qi Tian. Video super-resolution with temporal group attention. In *CVPR*, 2020. 5

[14] Takashi Isobe, Fang Zhu, and Shengjin Wang. Revisiting temporal modeling for video super-resolution. In *BMVC*, 2020. 1, 2, 5

[15] Younghyun Jo, Seoung Wug Oh, Jaeyeon Kang, and Seon Joo Kim. Deep video super-resolution network using dynamic upsampling filters without explicit motion compensation. In *CVPR*, 2018. 5

[16] Nan Rosemary Ke, Anirudh Goyal, Olexa Bilaniuk, Jonathan Binas, Michael C Mozer, Chris Pal, and Yoshua Bengio. Sparse attentive backtracking: Temporal creditassignment through reminding. In *NIPS*, 2018. 2

[17] Wenbo Li, Xin Tao, Taian Guo, Lu Qi, Jiangbo Lu, and Jiaya Jia. MuCAN: Multi-correspondence aggregation network for video super-resolution. In *ECCV*, 2020. 5

[18] Tsungnan Lin, Bill G Horne, Peter Tino, and C Lee Giles. Learning long-term dependencies in NARX recurrent neural networks. *IEEE Transactions on Neural Networks*, 1996. 2

[19] Ce Liu and Deqing Sun. On bayesian adaptive video super resolution. *TPAMI*, 2014. 4, 5

[20] Contributors MMEditing. MMEditing: OpenMMLab Image and Video Editing Toolbox, 3 2022. 5

[21] Seungjun Nah, Sungyong Baik, Seokil Hong, Gyeongsik Moon, Sanghyun Son, Radu Timofte, and Kyoung Mu Lee. NTIRE 2019 challenge on video deblurring and super-resolution: Dataset and study. In *CVPRW*, 2019. 4, 5

[22] Seungjun Nah, Sanghyun Son, and Kyoung Mu Lee. Recurrent neural networks with intra-frame iterations for video deblurring. In *CVPR*, 2019. 2

[23] Simon Niklaus and Feng Liu. Softmax splatting for video frame interpolation. In *CVPR*, 2020. 2

[24] Mehdi S M Sajjadi, Raviteja Vemulapalli, and Matthew Brown. Frame-recurrent video super-resolution. In *CVPR*, 2018. 1, 2, 5

[25] Rohollah Soltani and Hui Jiang. Higher order recurrent neural networks. *arXiv preprint arXiv:1605.00064*, 2016. 2

[26] Ke Sun, Yang Zhao, Borui Jiang, Tianheng Cheng, Bin Xiao, Dong Liu, Yadong Mu, Xinggang Wang, Wenyu Liu, and Jingdong Wang. High-resolution representations for labeling pixels and regions. *arXiv preprint arXiv:1904.04514*, 2019. 2

[27] Xin Tao, Hongyun Gao, Renjie Liao, Jue Wang, and Jiaya Jia. Detail-revealing deep video super-resolution. In *CVPR*, 2017. 5

[28] Yapeng Tian, Yulun Zhang, Yun Fu, and Chenliang Xu. TDAN: Temporally deformable alignment network for video super-resolution. In *CVPR*, 2018. 1, 2, 4

[29] Hua Wang, Dewei Su, Longcun Jin, and Chuangchuang Liu. Deformable non-local network for video super-resolution. *IEEE Access*, 2019. 2, 4

[30] Jingdong Wang, Ke Sun, Tianheng Cheng, Borui Jiang, Chaorui Deng, Yang Zhao, Dong Liu, Yadong Mu, Mingkui Tan, Xinggang Wang, Wenyu Liu, and Bin Xiao. Deep high-resolution representation learning for visual recognition. *TPAMI*, 2020. 2

[31] Xintao Wang, Kelvin C.K. Chan, Ke Yu, Chao Dong, and Chen Change Loy. EDVR: Video restoration with enhanced deformable convolutional networks. In *CVPRW*, 2019. 1, 2, 4, 5, 6

[32] Xintao Wang, Liangbin Xie, Chao Dong, and Ying Shan. Real-ESRGAN: Training real-world blind super-resolution with pure synthetic data. In *ICCVW*, 2021. 8

[33] Xiaoyu Xiang, Yapeng Tian, Yulun Zhang, Yun Fu, Jan P Allebach, and Chenliang Xu. Zooming Slow-Mo: Fast and accurate one-stage space-time video super-resolution. In *CVPR*, 2020. 2

[34] Xiangyu Xu, Muchen Li, Wenxiu Sun, and Ming-Hsuan Yang. Learning spatial and spatio-temporal pixel aggregations for image and video denoising. *TIP*, 2020. 4

[35] Tianfan Xue, Baian Chen, Jiajun Wu, Donglai Wei, and William T Freeman. Video enhancement with task-oriented flow. *IJCV*, 2019. 1, 4, 5, 6

[36] Ren Yang, Radu Timofte, Jing Liu, Yi Xu, Xinjian Zhang, Minyi Zhao, Shuigeng Zhou, Kelvin CK Chan, Shangchen Zhou, Xiangyu Xu, et al. NTIRE 2021 challenge on quality enhancement of compressed video: Methods and results. In *CVPRW*, 2021. 8

[37] Peng Yi, Zhongyuan Wang, Kui Jiang, Junjun Jiang, and Jiayi Ma. Progressive fusion video super-resolution network via exploiting non-local spatio-temporal correlations. In *ICCV*, 2019. 4, 5

[38] Shangchen Zhou, Jiawei Zhang, Jinshan Pan, Haozhe Xie, Wangmeng Zuo, and Jimmy Ren. Spatio-temporal filter adaptive network for video deblurring. In *ICCV*, 2019. 2

[39] Xizhou Zhu, Han Hu, Stephen Lin, and Jifeng Dai. Deformable ConvNets v2: More deformable, better results. In *CVPR*, 2019. 2, 4

[40] Juntang Zhuang, Junlin Yang, Lin Gu, and Nicha Dvornek. ShelfNet for fast semantic segmentation. In *ICCVW*, 2019. 2